remote sensing

MDPI

Article

The Combined ASTER MODIS Emissivity over Land (CAMEL) Part 1: Methodology and High Spectral Resolution Application

E. Eva Borbas [1,*], Glynn Hulley [2], Michelle Feltz [1], Robert Knuteson [1] and Simon Hook [2]

[1] Space Science and Engineering Center, University of Wisconsin-Madison, Madison, WI 53706, USA; michelle.feltz@ssec.wisc.edu (M.F.); robert.knuteson@ssec.wisc.edu (R.K.)

[2] California Institute of Technology Jet Propulsion Laboratory, Pasadena, CA 91109, USA; Glynn.Hulley@jpl.nasa.gov (G.H.); Simon.Hook@jpl.nasa.gov (S.H.)

* Correspondence: eva.borbas@ssec.wisc.edu; Tel.: +1-608-263-0228

Received: 28 February 2018; Accepted: 12 April 2018; Published: 21 April 2018

Abstract: As part of a National Aeronautics and Space Administration (NASA) MEaSUREs (Making Earth System Data Records for Use in Research Environments) Land Surface Temperature and Emissivity project, the Space Science and Engineering Center (UW-Madison) and the NASA Jet Propulsion Laboratory (JPL) developed a global monthly mean emissivity Earth System Data Record (ESDR). This new Combined ASTER (Advanced Spaceborne Thermal Emission and Reflection Radiometer) and MODIS (Moderate Resolution Imaging Spectroradiometer) Emissivity over Land (CAMEL) ESDR was produced by merging two current state-of-the-art emissivity datasets: the UW-Madison MODIS Infrared emissivity dataset (UW BF) and the JPL ASTER Global Emissivity Dataset Version 4 (GEDv4). The dataset includes monthly global records of emissivity and related uncertainties at 13 hinge points between 3.6–14.3 μm, as well as principal component analysis (PCA) coefficients at 5-km resolution for the years 2000 through 2016. A high spectral resolution (HSR) algorithm is provided for HSR applications. This paper describes the 13 hinge-points combination methodology and the high spectral resolutions algorithm, as well as reports the current status of the dataset.

Keywords: emissivity; infrared; surface; land; hyperspectral; radiation

1. Introduction

Land Surface Temperature and Emissivity (LST&E) data are critical variables for studying a variety of Earth surface processes and surface–atmosphere interactions such as evapotranspiration, surface energy balance, and water vapor retrievals. LST&E have been identified as an important Earth System Data Record (ESDR) by National Aeronautics and Space Administration (NASA) and many other international organizations (NASA Strategic Roadmap Committee #9, 2005; Global Climate Observing System (GCOS), 2003; Climate Change Science Program (CCSP), 2006 and the recently established International Surface Temperature Initiative) [1].

Accurate knowledge of LST&E at high spatial (1 km) and temporal (hourly) scales is a key requirement for many energy balance models to estimate important surface biophysical variables such as evapotranspiration and plant-available soil moisture [2,3]. LST&E data are essential for balancing the Earth's surface radiation budget. For example, a surface emissivity error of 0.1 will result in climate models having errors of up to 7 Wm^{-2} in their upward long-wave radiation estimates, which is a much larger term than the surface radiative forcing (~2–3 Wm^{-2}) due to an increase in greenhouse gases [4]. LST&E are also used to monitor land-cover/land-use changes [5], and in atmospheric retrieval schemes [6].

LST&E products are generated with accuracies that vary depending on the input data, including ancillary data such as atmospheric water vapor, as well as algorithmic approaches. For example, certain Moderate Resolution Imaging Spectroradiometer (MODIS) products (MOD11) use an infrared (IR) split window algorithm applied to two or more bands in conjunction with an emissivity estimate based on the land classification to produce the LST. Conversely, other MODIS products (MOD21) [7] use a physics-based approach involving a radiative transfer model to first correct the data to a surface radiance, and then use a model to extract the temperature and emissivities in the spectral bands. This physics-based approach is also adopted for the Advanced Spaceborne Thermal Emission and Reflection Radiometer (ASTER) measurements. Validation of these approaches has shown that they are complementary, with the split-window approach better suited over heavily vegetated regions, and the physics-based approach better suited for semi-arid and arid regions. Figure 1 shows an example of the ASTER Global Emissivity Dataset Version 3 (ASTER GEDv3) [8] and the UW-Madison MODIS Infrared emissivity dataset Baseline Fit (UW BF) [9] mean emissivity at 9.1 µm over Africa for the summer season (July–September) between 2000 and 2008. There is good overall agreement between the two databases; however, each has their own benefits and drawbacks. For example, the ASTER GEDv3 is able to better capture the deeper quartz minimum at 9.1 µm compared to the UW BF, which has only one band available in this region (MODIS band 29, 8.5 µm). For the UW BF database, the emissivity in the mid to long-wave region (8–12 µm) is not well defined, because MODIS only has three bands in this region (bands 8.5 µm, 11 µm, and 12 µm). This results in an imperfect spectral shape in the two quartz doublet regions at 8.5 µm and 12 µm. The advantages of the UW BF include its moderate spatial resolution (5 km), its uniform temporal coverage (monthly), and that its emissivities span the entire IR region (3.6–12 µm). In contrast, although there are more bands in the ASTER GEDv3 available to define the spectral shape in the mid–long IR region (five bands, bands at 8.3 µm, 8.6 µm, 9.3 µm, 10.6 µm, and 11.3 µm), there are no bands in the short-wave infrared (SWIR) region around 3.8–4.1 µm, which limits its use in models and other atmospheric retrieval schemes. On the plus side, ASTER GEDv3 has high spatial resolution (~100 m) and high accuracy over arid regions. In terms of temporal sampling, the MODIS product has been used to create monthly emissivity estimates, whereas constraints on the ASTER data collection limit the derived emissivity dataset to multi-year climatologies. By combining the two measurements, the Combined ASTER and MODIS Emissivity over Land (CAMEL) dataset takes advantage of the strengths of each dataset while mitigating the problems of each.

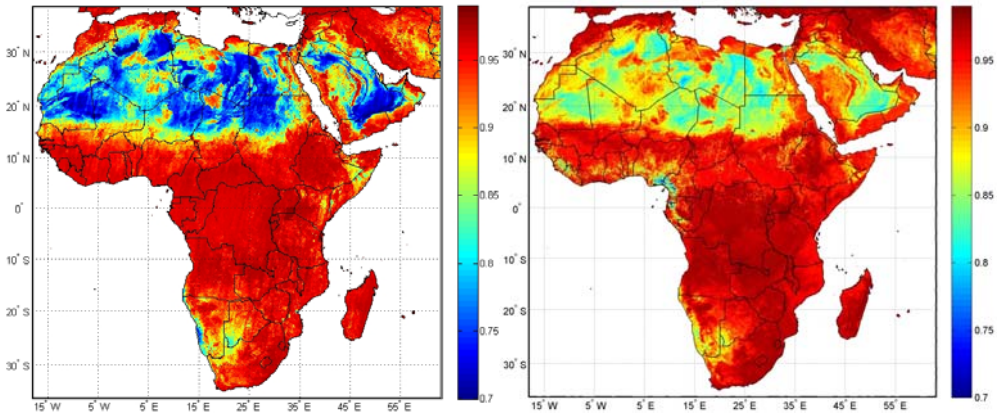

Figure 1. (**Left**) Advanced Spaceborne Thermal Emission and Reflection Radiometer Global Emissivity Dataset (ASTER GEDv3) mean summertime (July–September) emissivity for band 12 (9.1 µm), (**Right**) UW-Madison MODIS Infrared emissivity dataset Baseline Fit emissivity (UW BF) mean summertime (July–September) emissivity at 9.1 µm, which is the same as Moderate Resolution Imaging Spectroradiometer (MODIS) Band 29, 8.5 µm.

NASA has recognized the importance of LST&E, and identified the need to develop long-term, consistent, and calibrated data and products that are valid across multiple missions and satellite sensors. Under the NASA Making Earth Science Data Records for Use in Research Environments (MEaSUREs) program, a monthly mean unified Low Earth Orbit (LEO) based Land Surface Emissivity (LSE) ESDR at 5 km has been produced by merging two current state-of-the-art emissivity databases, the UW-Madison MODIS based UW BF, and the Jet Propulsion Laboratory (JPL) ASTER GED Version4 (GEDv4) [10], which is called the CAMEL. The CAMEL LSE ESDR has been further extended to hyperspectral resolution using a Principal Component (PC) regression approach similar to the UW high spectral resolution (HSR) algorithm [11].

This document is the first part of a two-part series that will describe the NASA MEaSUREs LSE ESDR called CAMEL Version 1.0 [12] in detail, including their methodologies, data products, and technical aspects. Part II discusses the uncertainty determination and current validation efforts of the CAMEL database.

2. Data

In this section, the two input emissivity databases are introduced: the ASTER GEDv4 and the UW BF emissivity, along with the selected laboratory measurements that are needed for HSR application.

2.1. The ASTER Global Emissivity Dataset

In 2009, a level-3 mean, gridded ASTER Global Emissivity Dataset Verison3 (ASTER GEDv3) was generated using all ASTER clear-sky data available since 2000. The emissivity retrieval was based on an improved Temperature Emissivity Separation (TES) algorithm with a water vapor scaling (WVS) atmospheric correction approach [13,14]. The ASTER GEDv3 is output on $1^\circ \times 1^\circ$ grids at 100-m, 1-km, and 5-km spatial resolutions. The product has been validated extensively over a set of pseudo-invariant sites, and results indicate agreement to within 1.5% [15]. Additionally, ASTER GEDv3 has shown good agreement with other coarser sensor LSE products such as Atmospheric Infrared Sounder (AIRS) [16] and MODIS [13,17]. The ASTER GEDv3 is currently being distributed at the NASA Land Processes Distributed Active Archive Center (LP DAAC) at the U.S. Geological Survey (USGS) Earth Resources Observation and Science (EROS) with global coverage, and has been available since the end of 2012.

2.1.1. ASTER Vegetation and Snow Cover Adjustment

Since the ASTER GEDv3 product represents a mean emissivity climatology of ASTER data acquired over an 11-year period (2000–2010), an emissivity adjustment is necessary over heterogeneous land cover types that are subject to annual and inter-annual land cover changes (e.g., due to snow and ice melt, and agricultural practices). The emissivity of vegetation and snow is fairly high and constant (~0.98–1.0). As a result, surfaces with high amounts of vegetation or snow cover reduce the amount of spectral variation. This relationship is used to adjust the ASTER GEDv3 emissivity product by either increasing or decreasing the spectral contrast as a simple function of the amount of snow or vegetation relative to the reference mean state. The methodology to create the vegetation and snow adjusted ASTER GEDv4 emissivity is described in Hulley et al. [14]. This allows the ASTER GEDv4 emissivity product to be produced at the same monthly resolution of the UW products. The snow cover amount is obtained from the standard MODIS snow cover maps (MOD10 product). The vegetation amount is obtained by applying the National Oceanic and Atmospheric Administration (NOAA) National Environmental Satellite, Data and Information Service (NESDIS) "Green Vegetation Fraction" approach to the NASA MOD13A3 monthly gridded normalized difference vegetation index (NDVI) product, whereby the current vegetation influence is estimated as f = (NDVI_current - NDVI_min)/(NDVI_max - NDVI_min) [18]. The NDVI is a well-tested and proven indicator of partial and emerging vegetation growth.

2.1.2. Aggregation of ASTER GED to 5-km Resolution

The ASTER GEDv3 is produced in 1° × 1° grids with a resolution of 0.001° (~100 m), and consequently, the spectral emissivities are first aggregated to the UW database resolution of 0.05° (5 km) before merging. It has been shown that a simple aggregation from fine to coarse resolution is valid only if the scene is homogeneous in emissivity and surface temperature [19]. In this case, the effective emissivity is simply an average of individual pixels, *i*. $\bar{\varepsilon}(\nu) = 1/n \sum \varepsilon(i,\nu)$ *i*=1:*n*, where $\bar{\varepsilon}(\nu)$ is the effective spectral emissivity for wavelength ν at the coarser resolution scale, and $\varepsilon(i,\nu)$ is the spectral emissivities for each pixel *i* at the finer resolution scale. This approach was used successfully in validating AIRS emissivities with the ASTER emissivity product over large homogenous sand seas [16]. However, over more heterogeneous cover types, this assumption breaks down due to a higher variability in the surface temperature distribution. A potential solution is to aggregate the surface emitted radiance for each pixel at the finer resolution scale (e.g., ASTER at 100 m), and then normalize with the radiance of an effective surface temperature at the coarser pixel scale (e.g., MODIS at 5 km), as follows:

$$\bar{\varepsilon}_\nu = \frac{\frac{1}{n}\sum_{i=1}^{n} \varepsilon_{i,\nu} \cdot B_\nu(T_{i,s})}{B_\nu(\overline{T_s})} \quad (1)$$

where $B_\nu(T_{i,s})$ is the radiance for temperature $T_{i,s}$ for each pixel *i* at the finer resolution scale, and $B_\nu(\overline{T_s})$ is the radiance for an effective temperature $\overline{T_s}$ at the coarser resolution scale. This method was used to intercompare emissivities from the ASTER GEDv4 with MODIS emissivities at a coarser scale over the southwestern United States (USA) [17].

The MODIS products known as MOD11C3 and ASTER GEDv4 are both level-3 gridded products. Since both the original pixel resolution of the ASTER GEDv3 (100 m) and MODIS (1 km) are resampled to 0.05 degree, any misregistration and geolocation inconsistencies between ASTER/MODIS are very likely to be negligible, particularly for thermal data. In addition, ASTER's geometric accuracy and pixel geolocation knowledge have exceeded the original goals of the project [20]. For Terra and Aqua MODIS instruments, specific correction approaches are implemented to ensure that the geolocation of individual MODIS observations are at the sub-pixel accuracy level [21]. Additionally, the MODIS Terra and Aqua band-to-band registration accuracy is under 50 m [22,23].

2.2. The UW Baseline Fit and High Spectral Resolution Land Surface Emissivity Database

At the University of Wisconsin-Madison, a monthly MODIS global IR land surface emissivity database (UW BF) was developed based on the standard monthly mean MODIS emissivity product at 10 wavelengths (3.6, 4.3, 5.0, 5.8, 7.6, 8.3, 9.3, 10.8, 12.1, and 14.3 μm) at 5-km spatial resolution. The baseline fit method [24], which was based on a conceptual model developed from laboratory measurements of surface emissivity, is applied to fill in the spectral gaps between the six available MODIS/MYD11 emissivity bands. The 10 wavelengths in the UW BF emissivity database were chosen as hinge points to capture as much of the shape of the higher resolution emissivity spectra as possible. This approach was extended by the method described in Borbas [11] and Masiello et al. [25] to provide 416 spectral points from 3.6 μm to 14.3 μm. The UW HSR emissivity algorithm is based on a principal component analysis (PCA) regression using the eigenfunction representation of high spectral resolution laboratory measurements from the ASTER spectral library [26].

In the next section, the input data for the UW database are discussed. The quality and accuracy of those input data is important for determining the uncertainty of the CAMEL dataset.

Input MODIS MOD11 Products

The operational MODIS MOD11 surface temperature and emissivity products are generated over land in clear-sky conditions for day and night in 5-min granules for both NASA's Earth Observing System (EOS) Terra and Aqua satellites. The 5-min granule products are averaged to daily, eight-day, and monthly time scales, and the Level-3 gridded products are produced at 5-km spatial resolution.

The UW BF emissivity data is comprised of the monthly mean surface emissivity products (MOD11C3) that include IR land surface emissivity at six IR bands (20, 22, 23, 29, 31, and 32) located in the 3.6–4.2 μm and the 8–13 μm atmospheric windows. The approach to derive the monthly mean land surface temperature and emissivity assumes emissivity, which is known as the day–night algorithm [27], does not change between day and night at the same location over a period of a few days. This assumption is one of the sources of uncertainty for the CAMEL product. The Collection 4.0/4.1 (Col 4.0/4.1) MOD11C3 products are used as input to the UW BF database, even though newer Collections (Col 5 and 6) have been released since then. We have found that the Col 4.0/4.1 version has the best quality products. Significant differences were found between the MYD11 Col 4 and 5 data: higher emissivity values at the reststrahlen band over desert areas (see Figure 2); an increase in minimum emissivity for bands 20, 22, 23, and 29 (3.7μm, 3.9 μm, 4.0 μm, and 8.5 μm, respectively) by ~0.1; and a loss of variability for bands 31 and 32 (11 μm and 12 μm, respectively).

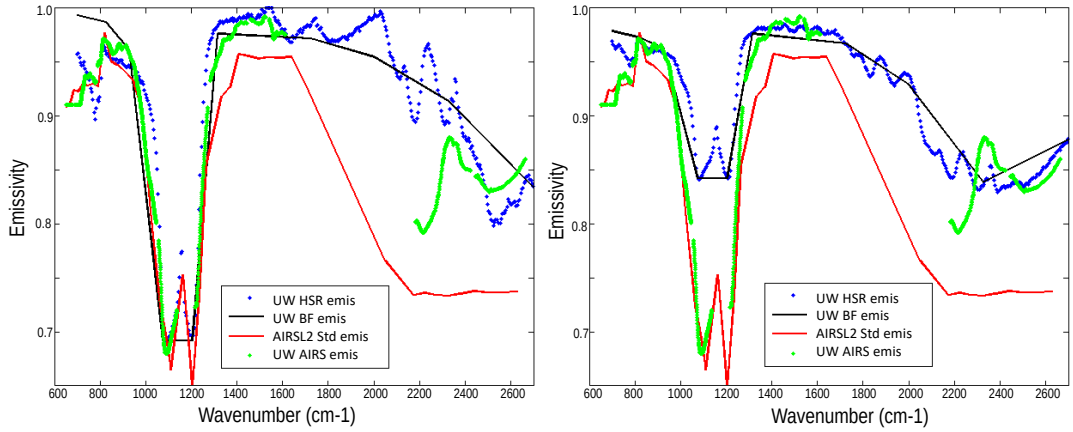

Figure 2. Emissivity comparison on January 2003 over Sahara Desert (Lat = 25.075N, Lon = 26.058E) of UW BF (solid black line), UW high spectral resolution (HSR) (blue dots), the AIRS L2 (V5.0) Standard products (red line), and the UW/AIRS (green dots) emissivity products. (**Left**) The UW BF and UW HSR emissivity products have been derived from the Col 4, and (**Right**) from the Col 5 MODIS emissivity products.

Due to these differences, the NASA LP DAAC decided in the beginning of 2007 to continue to produce Col 4 data beyond December 2006, but using the only available Col 5 MODIS input data such as the cloud mask, L1B data, and atmospheric profiles. This version of the MYD11 data is called Col 4.1. More information about the MYD11 Col 4.1 product may be found in the C4.1 LST Document [28]. The update (mostly due to the changes in the cloud mask) between Col 4 and Col 4.1 in January 2007 caused minimal inconsistencies in the UW BF database (see left panels of Figure 3.).

The processing of the MOD11C3 Col 4.1 and 5 products was discontinued in 2017 and replaced by a new Col 6 product. Figure 3 shows a time series comparison of Col 4/4.1 (left, currently used as input to UW BF) and Col 6 (right) for bands 20, 29, 31, and 32 MO/YD11C3 monthly mean emissivity products for Aqua (red) and Terra (blue) MODIS over a Namib desert location. The Col 6 band 20 (3.76 μm) and band 29 (8.5 μm) emissivity are—we believe—mistakenly identical for both Terra and Aqua MODIS. It appears that band 29 values have been copied into the band 20 variable. Bands 31 and 32 show very little time variation. These facts make the Col 6 MOD11C3 emissivity data unusable for our project. Despite the Col 4/4.1 MOD11 products being the best quality for our purposes, there are some problems in that dataset as well for longer time-scale purposes. The increasing emissivity of the Terra band 29 was probably due to the band 29 cross-talk error [29]. This will likely be mitigated in the future by reprocessing the data on the Col 6.1 L1B cross-talk corrected radiances. Col 4.1 emissivity values also start to decrease significantly, especially for the long-wave region, starting in 2009 January, which is an issue in the UW BF emissivity database. This artifact may be caused by an initialization

issue during processing. This defect is eliminated by ASTER GEDv4 data in the CAMEL database, which is presented in Figure 4.

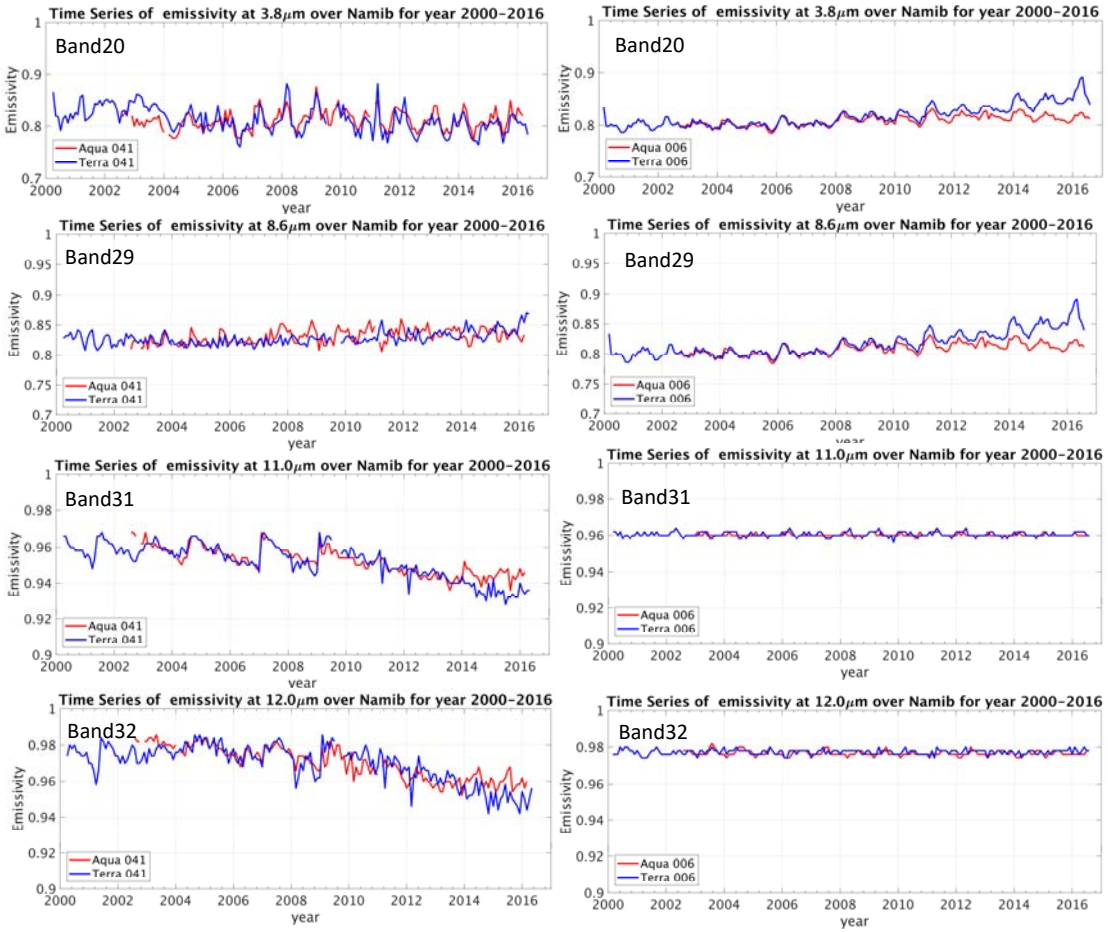

Figure 3. Time series of Col 4/4.1 (**left**) and Col 6 (**right**) band 20, 29, 31, and 32 MxD11C3 monthly mean emissivity for Aqua (red) and Terra (blue) MODIS over a Namib desert location (Lat: 24.25S, Lon:15.25E). Note: In Col 6, band 20 appears to be a copy of band 29 for both Terra and Aqua MODIS.

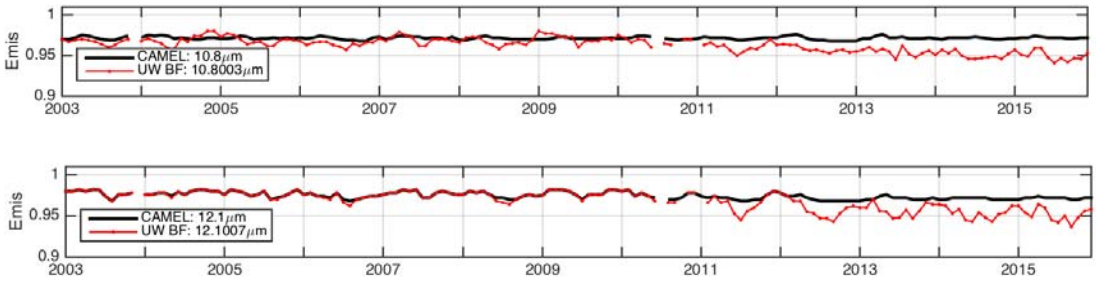

Figure 4. Time series of the Combined ASTER and MODIS Emissivity over Land (CAMEL) database and its input UW BF dataset at 10.8 μm (**top panel**) and 12.1 μm (**bottom panel**) is shown over the Atmospheric Radiation Measurement (ARM) Southern Great Plains (SGP) Cart Site. The CAMEL algorithm effectively eliminates the emissivity degradation observed after 2009 for the long-wave MODIS MOD11 product based UW BF hinge-points.

2.3. The Laboratory Measurements

The CAMEL HSR algorithm takes advantage of a wide variety of laboratory measurements of terrestrial materials (minerals, soils, vegetation, fresh water, salt water, snow, ice, etc.) that have been collected at high spectral resolution for a continuous IR range [30,31]. The laboratory measurements have the advantage of being performed using short path lengths and under purged conditions to minimize the effects of water vapor absorption (and other gases). They also take advantage of laboratory spectrometers that have resolving powers of 1000 or more. The laboratory measurements used to derive the emissivity in this paper were drawn from the MODIS emissivity library (http://www.icess.ucsb.edu/modis/EMIS/html/em.html) at the University of California, Santa Barbara, and the ASTER spectral library [26], including spectra from the John Hopkins University (JHU) Spectral Library, the JPL Spectral Library, and the United States (U.S.) Geological Survey (USGS) Spectral Library.

The MEaSUREs CAMEL database was extended to high spectral resolution using a PC regression analysis similar to the UW HSR algorithm. While the UW HSR algorithm includes 123 selected laboratory measurements, the CAMEL HSR algorithm now includes three sets of laboratory spectra, specifically 55 selected spectra (called version 8) for general use, 82 spectra (called version 10; version 8 + carbonates) for non-vegetated cases, and four snow/ice selected spectra (version 12). The three sets of CAMEL laboratory data and the UW HSR 123 selected laboratory measurements are presented in Figure 5. If the snow fraction is larger than 0.5, only the new snow/ice set of PCs based on laboratory measurements is used. The three new sets of laboratory sets better characterize the emissivity spectra of the non-vegetated surface types and snow-covered areas.

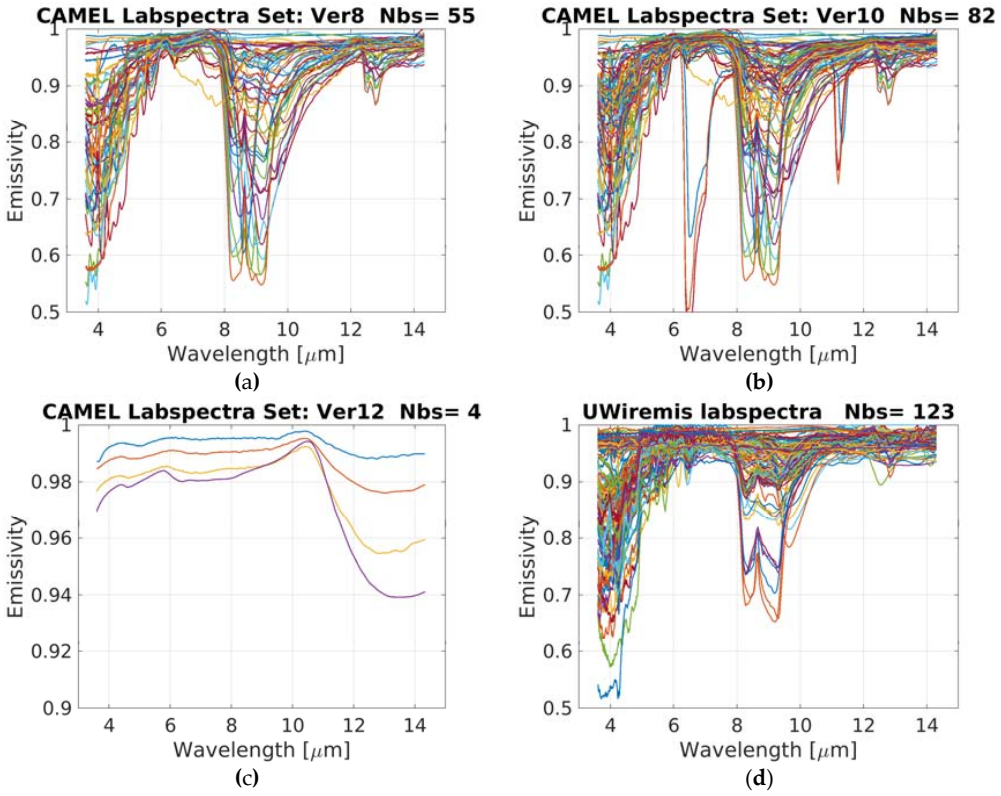

Figure 5. The CAMEL high spectral resolution (HSR) emissivity algorithm now includes three sets of laboratory spectra: (**a**) 55 selected spectra for general use (called version 8), (**b**) 82 spectra for surface types including carbonates (called version 10; version 8 + carbonates), and (**c**) four snow/ice selected spectra (version 12). The UW HSR 123 selected laboratory measurements (**d**) are shown for comparison.

3. Method

As noted earlier, CAMEL is produced by combining the UW-Madison MODIS based UW BF database and the JPL ASTER GEDv4. A limitation of the UW BF database is that emissivity in the thermal IR region (TIR) region (8–12 μm) is not well defined, because MODIS only has three bands in this region (bands 29, 31, 32). This results in an imperfect TIR spectral shape in the two quartz doublet regions at 8.5 μm and 12 μm. The advantages are its moderate spatial resolution (5 km), uniform temporal coverage (monthly), and emissivities, which span the entire IR region (3.6–12 μm). A disadvantage of the ASTER GED is that although there are more bands to define the spectral shape in the TIR region (five bands, 8–12 μm), there are no bands in the mid-wave infrared (MIR) region around 3.8–4.1 μm, which limits its use in models and other atmospheric retrieval schemes. The advantages are its high spatial resolution (~100 m) and high accuracy over arid regions. The two datasets have been integrated together to capitalize on the unique strengths of each product's characteristics. This integration involved two preparatory steps: (1) ASTER GEDv3 emissivities are adjusted for vegetation and snow cover variations over heterogeneous regions to produce ASTER GEDv4, (2) ASTER GEDv3 emissivities are aggregated from 100-m resolution to the UW BF 5-km resolution, and two processing steps: (i) the spectral emissivities are merged together to generate the CAMEL product at 13 hinge points from 3.6 μm to 12 μm, and (ii) the 13 hinge points have been further extended to hyperspectral resolution using a PC-regression approach. The preparation of the ASTER data in steps 1 and 2 has been discussed in Sections 2.1.1 and 2.1.2. The two processing steps are summarized in Figure 6, and are discussed below in more detail.

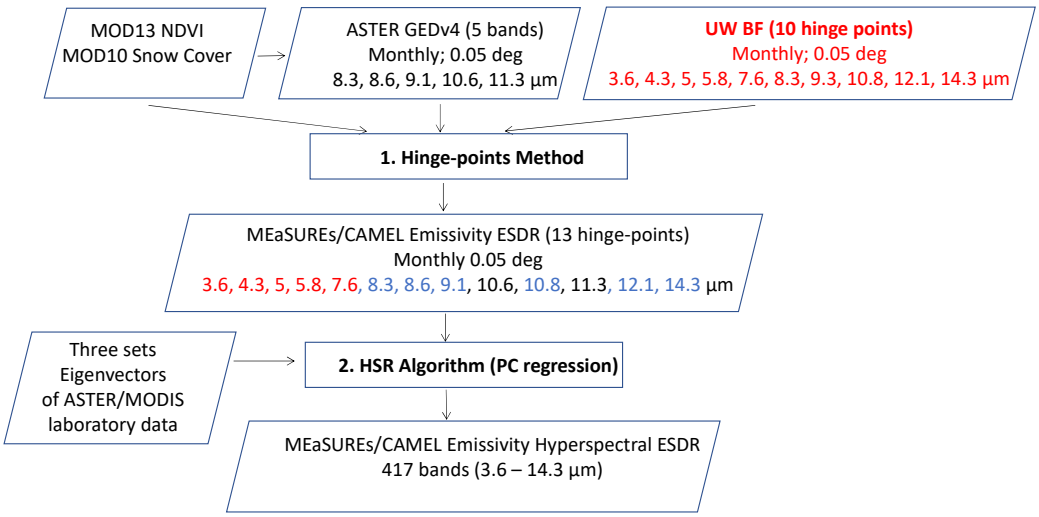

Figure 6. Making Earth System Data Records for Use in Research Environments (MEaSUREs) CAMEL Emissivity Earth System Data Record (ESDR) flowchart.

3.1. Emissivity Hinge-Points Methodology

The merging of the spectral emissivities from the five ASTER bands with the 10 hinge-point bands from the UW BF database and the determination of the CAMEL emissivity hinge points are summarized in Table 1, and described below.

CAMEL hinge points between 3.6–7.6 μm: In the ASTER band gap of the SWIR and MIR region, the CAMEL emissivities between 3.6–7.6 μm are determined by the UW BF values only, and keep the location of the hinge points.

CAMEL hinge points at 10.6 μm and 11.3 μm: The 10.6 μm and 11.3 μm hinge points are added based on the additional observations from ASTER band 10.6 μm and 11.3 μm. CAMEL values at these hinge points are determined from the ASTER GEDv4 observations only.

Table 1. Method to create CAMEL emissivity for the 13 hinge points.

CAMEL Channel Number	CAMEL Wavelength [μm]	UWBF Channels	ASTER Channels	CAMEL Combining Method
1	3.6	Y	-	UWBF1
2	4.3	Y	-	UWBF2
3	5.0	Y	-	UWBF3
4	5.8	Y	-	UWBF4
5	7.6	Y	-	UWBF5
6	8.3	Y	Y	ASTER1 + (CAMEL7(UWBF6, ASTER2) − ASTER2)
7	8.6	Y	Y	Weighted Mean(UWBF6, ASTER2)
8	9.1	-	Y	ASTER 3 + (CAMEL7(UWBF6, ASTER2) − ASTER2)
9	10.6	-	Y	ASTER4
10	10.8	-	-	Linear Interpolation(ASTER4, ASTER5)
11	11.3	-	Y	ASTER5
12	12.1	Y	-	UWBF9 but if ASTER5 > BF9, UWBF9 + diff(UWBF9, ASTER5) * weight if snowfrac > 0.5
12 *	12.1	Y	-	UWBF9 + diff(CAMEL10, UWBF8)
13	14.3	Y	-	UWBF10 but if ASTER5 > BF9, UWBF9+ diff(UWBF9, ASTER5) * weight if snowfrac > 0.5
13 *	14.3	Y	-	CAMEL12

* CAMEL channels 12 and 13 have separate combining methods based on whether the pixel is defined as snow or non-snow using 0.5 snow fraction as a threshold.

CAMEL hinge point at 8.6 μm: This is the only hinge point where the MODIS band 29 (8.55 μm) and ASTER band 11 (8.6 μm) overlap; both have very similar spectral response functions. Since these two bands match closely, we used a weighting rule based on the uncertainties using a "combination of states of information" approach. In this approach, two pieces of information (e.g., two spectral emissivities $\varepsilon(1,\nu)$ and $\varepsilon(2,\nu)$ can be merged in a probabilistic manner by weighting each input based on its relative uncertainty, i.e., $\varepsilon(\nu) = [1/(w1 + w2)]\ [w1{\cdot}\varepsilon(1,\nu) + w2{\cdot}\varepsilon(2,\nu)]$, where w is a weighting factor based on an uncertainty, σ, as follows: $w = 1/\sigma$. To apply this method, we used 90% and 10% weights as the corresponding uncertainties for ASTER GEDv4 and UW BF on a pixel-by-pixel basis. Given the lack of uncertainty estimates in the MODIS (MOD11) product, the 90/10% weights are determined based on test case studies. In the future, when uncertainty estimates of the MODIS products are available, those weights will be adjusted and objectively defined based on the uncertainties in the input products (MODIS and ASTER). Since the ASTER GEDv4 has more bands that more accurately define the quartz doublets, ASTER band 11 (8.6 μm) gets the 90% weight for arid and semi-arid regions, while for all of the other cases, the UW BF hinge point 6 (8.3 μm) is weighted by the 90%. To determine the arid and semi-arid region, the ASTER NDVI (< 0.2) and ASTER 9.1-μm band ($\leq$0.85) is used. Additionally, over the heavily vegetated tropical rainforests, the MODIS MOD11 emissivity suffers from cloud contamination, resulting in a low emissivity value at the reststrahlen band. To avoid this artifact over this region ($\pm$20 degree latitude band where ASTER NDVI is larger than 0.7 and UW BF emissivity at 8.6 μm is less than 0.96), the ASTER 11 (8.6 μm) is weighted by 90%.

CAMEL hinge points at 8.3 μm and 9.1 μm: The baseline fit procedure that was used in generating the UW BF product extends emissivity from MODIS band 29 (8.6 μm) to inflection points at 8.3 μm and 9.1 μm. The location of these inflection points was maintained, but the UW BF emissivities are improved by replacing the interpolated inflection points with retrieved ASTER emissivities from corresponding bands 10 (8.3 μm) and 12 (9.1 μm), and then adjusting them by the emissivity difference between the new CAMEL 8.6 μm and ASTER 8.6 μm bands. This significantly improves the spectral shape in the Si-O stretching region (8–12 μm).

CAMEL hinge point 10.8 μm: The CAMEL emissivity at the 10.8-μm hinge point is determined as the linear combination of the ASTER band 10.6 μm and 11.3 μm emissivity.

CAMEL hinge points at 12.1 μm and 14.3 μm: The UW BF emissivities at 12.1 μm and 14.3 μm are adjusted by the differences between the UW BF 12.1 μm and ASTER 11.3 μm emissivities to be

consistent with the 10.6–11.3 µm region (mostly ASTER-based observations) and improve the spectral shape in this TIR spectral region. A weighting factor is applied based on the difference between the UW BF 12.1 µm and ASTER 11.3 µm emissivities. If the UW BF emissivity value at 12.1 µm is larger than the value at ASTER 11.3 µm, it is likely that the input MOD11 data is not degraded (as is shown on the bottom panel of Figure 4 before 2011), and the weighting factor is 0, with no need for adjustment. If the difference is negative, suggesting that the UW BF 12.1 µm emissivity has likely degraded, so it is smaller than the ASTER 11.3 µm values, then the weighting factor varies based on the ASTER 11.3 µm emissivity value. The weighting factor is 1 or 2, depending on if the ASTER GEDv4 value is larger (likely vegetated or snow/ice covered surface) or smaller than 0.95 (likely mixed or unvegetated surface), respectively. If the weighting factor of 2 produces emissivity values larger than 1, the weighting factor is reduced to 1.5.

Figure 7 shows an example of how much the combined 8.6-µm CAMEL emissivity field differs from the input UW BF and ASTER GEDv4 data for February 2004. The CAMEL emissivity agrees with the UW BF data over vegetated areas (white area) and is higher (yellow-orange) for non-vegetated and snow-covered areas (see Figure 7d). Furthermore, the CAMEL emissivities agree with the ASTER GEDv4 emissivities over the arid, non-vegetated areas such as the Sahara Desert and Siberia (white areas), and is lower (blue) for vegetated scenes (See Figure 7e).

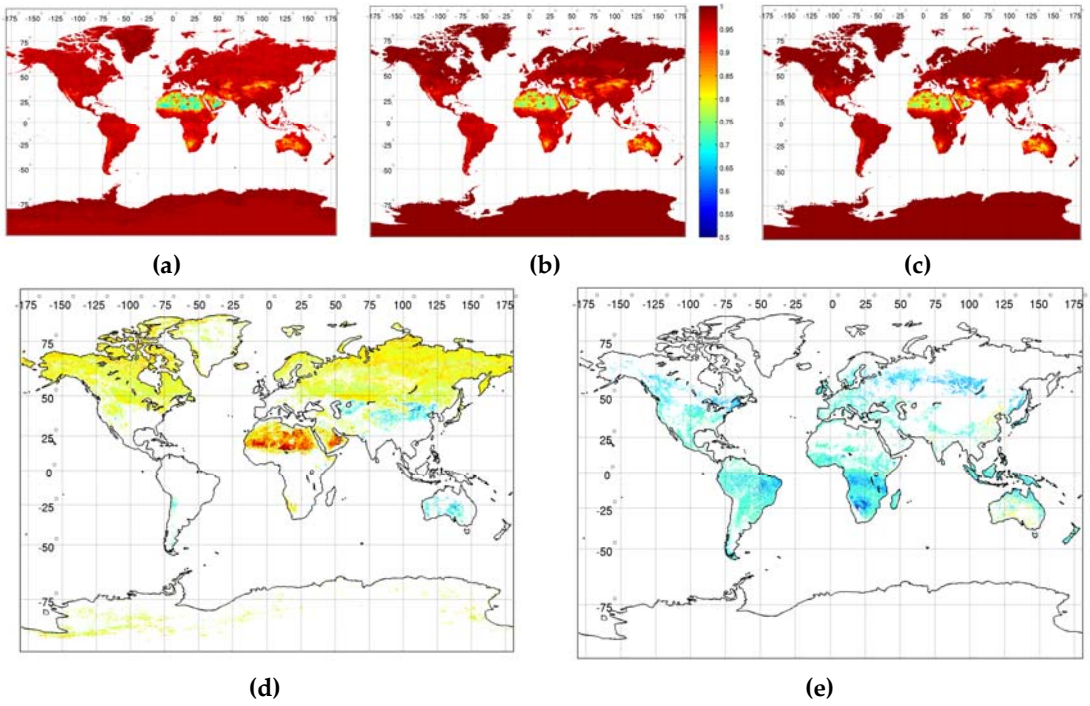

Figure 7. The UW BF (**a**), CAMEL (**b**) and the ASTER GEDv4 (**c**) emissivity at 8.6 µm for February 2004. The difference maps of the emissivity between CAMEL and UW BF database (**d**) and ASTER GED v4 (**e**) are also shown for February 2004.

3.2. High Spectral Resolution Methodology

The MEaSUREs CAMEL 13 hinge-point database was extended to high spectral resolution to capture the small-scale fluctuations in emissivity that were not captured by the CAMEL 13 hinge point dataset.

The CAMEL HSR algorithm uses a PC regression analysis, which is similar to the method developed for the UW HSR Algorithm [11,25]. We assume that emissivity can be derived as a linear combination of the first couple of eigenvectors (or principal components (PCs)) of the laboratory

measurements, and that the linear relationship between emissivity spectra and PCs are the same at both moderate and high spectral resolution.

The PCs (eigenvectors) are generated using three sets of selected laboratory measurements (chosen to represent various surface types), and are regressed to the CAMEL 13 hinge points as follows:

$$\vec{e} = \vec{c}\,U \tag{2}$$

where $\vec{e}[nh]$ is the CAMEL emissivity on 13 hinge points, $\vec{c}[npc]$ is the PCA coefficient vector, and $U[npc,nh]$ is the matrix of the PCs of the lab emissivity spectra on the reduced spectral resolution. The *nh* stands for the number of hinge points, which is 13 in our case, and *npc* is the number of eigenvectors. The coefficient can be calculated then:

$$\vec{c} = \vec{e}\,U^T\left(UU^T\right)^{-1} \tag{3}$$

After calculating the coefficients ($\vec{c}$), the high spectral resolution emissivity values are determined using Equation (2) at the same latitude and longitude point by using the high spectral resolution PCs of the laboratory sets. This time, the U matrix sizes are [*npc,nhsr*], where *nhsr* stands for the number of high spectral resolution wavenumber points.

In the HSR emissivity algorithm, the ($\vec{e}$) is actually the difference of the emissivity spectra from the mean (E_{lab}) of the selected laboratory dataset (e.g., "general", "general+carbonates", or "snow/ice"), so Equation (3) becomes:

$$\vec{c} = (\vec{e} - E_{lab})U^T\left(UU^T\right)^{-1} \tag{4}$$

Then, the high spectral resolution emissivity $\vec{e_h}$ is calculated:

$$\vec{e_h} = \vec{c}\,U_h + \vec{\lambda_h} \tag{5}$$

There are two primary updates in the CAMEL HSR algorithm from the UW HSR algorithm: one is the number of principal components (PCs) determination (this will be discussed in the next section), and the other is the selection of the laboratory measurements. While the UW HSR algorithm includes only one set of laboratory measurements for all of the surface types, the CAMEL HSR algorithm uses three sets of laboratory measurements based on the surface scene type and coverage: one for general purpose (55 spectra), one for arid areas, which includes more carbonate measurements (82 spectra), and a separate snow/ice set, which includes only snow and ice laboratory measurements (four spectra) (see Section 2.3 for more details). With these three separate categories, false spectral features have been avoided that occasionally occurred in the UW HSR emissivities. For example, the quartz doublet feature sometimes erroneously appeared over fully snow-covered areas.

Table 2 summarizes the methodology used to determine which laboratory set would be used for a given pixel. First, a carbonate test is performed that is based on the laboratory measurements. A pixel falls into the non-vegetated and carbonate category if the ASTER NDVI is less than 0.2, the CAMEL emissivity at 10.6 μm is larger than the 11.3 μm emissivity by more than 0.009, and the CAMEL emissivity in the SWIR region is lower than 0.9. If the carbonate test is true, the Version 10 laboratory dataset is assigned, and if it fails, then the "general" Version 8 laboratory dataset is assigned to the pixel. In the general category, the quartz doublet feature can be present, which requires more PCs to capture it accurately.

Table 2. Determination of the number of PCs and the version number of laboratory datasets for each pixel.

Tests	Version # of Laboratory Dataset	Number of PCs
[1]Carbonate test: yes	10 (general_carbonates)	5
[1]Carbonate test: no, but CAMEL9.1 <= 0.85	8 (general)	9
All the others	8 (general)	7
MOD10 snow fraction >= 0.5	12 (snow/ice)	2

[1]Carbonate test: $(CAMEL_{10.6} - CAMEL_{11.3}) > 0.009$ & ASTER NDVI < 0.2 & $CAMEL_{3.6} < 0.9$.

To determine the scene over a bare and sandy area, the 9.1-μm emissivity is used. If it is lower than 0.85, the surface probably contains quartz. Figure 8 shows an example of applying the PC regression fit to the CAMEL LSE ESDR product at 13 points over the Namib Desert, Namibia. Comparisons of the CAMEL emissivity with lab emissivity spectra from field sand samples show very good agreement, particularly in the quartz doublet regions at 8.5 μm and 12.5 μm when compared with the UW HSR. Biases and root mean square errors were reduced by 3% and 4%, respectively, by using the CAMEL product instead of the UW HSR product. This case failed the carbonate test, but the 9.1-μm CAMEL emissivity was less than 0.85; hence, the Version 8 (general) laboratory set with nine PCs was determined by the CAMEL HSR algorithm. The determination of the number of PCs is explained in more detail in the next section.

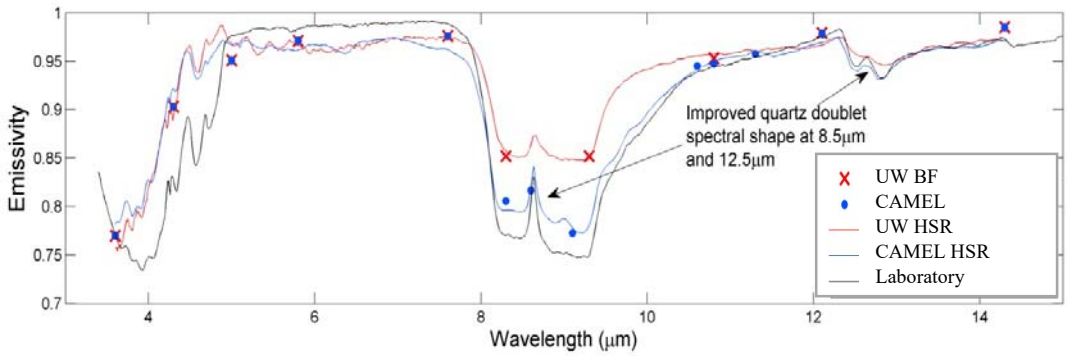

Figure 8. The advantages of combining the ASTER GEDv4 and UW BF databases are evident here, showing the emissivity spectra over the Namib Desert, Namibia. UW BF emissivity for January 2004 (crosses) and hyperspectral fit (red line), the CAMEL 13 hinge-point emissivity (blue dots) and hyperspectral fit (blue line), and lab spectra (black) of sand samples collected over the Namib Desert. Note the improved spectral shape in CAMEL HSR (blue) in the quartz doublet regions between 8–10 μm and 12–13 μm.

The snow fraction based on the MODIS MOD10 product has been added to the ASTER GEDv4, and hence to the CAMEL products, to improve the emissivity determination over snow and ice. In the CAMEL algorithm, if the snow fraction is larger than 0.5, then the snow/ice laboratory dataset (Version 12) is used with two PCs. The emissivity over fully snow and ice-covered areas is improved [32], but the 0.5 threshold assumption may need to be modified for partially snow/ice covered areas. A blended average emissivity between the snowy and not snowy emissivity spectra for a single pixel based on the snow fraction may be a better approach in the future.

Determining of the Number of Principal Components to Use

In the PCA regression method, the first PCs with the highest eigenvalues represent real variations in the data while the last, least significant PCs most often represent random white noise. In this study,

the maximum number of PCs allowed is 13, due to the number of spectral points of the input CAMEL hinge-point emissivities. However, use of the maximum number or close to the maximum number of PCs sometimes makes the solution unstable.

To determine the appropriate number of PCs to use, we first determine the percentage cumulative variance (PCV) function and eigenvalues of the three laboratory datasets. This was then followed by spectral reconstruction for the selected case sites, which were selected to cover the major global surface types, such as the sandy desert location over Namib (see also Figure 8), the rocky carbonated surface type over Yemen, seasonal vegetation cover at the Atmospheric Radiation Measurement (ARM) Cart site, a mountainous region at Mt. Massive, which is covered by forest and snow in the winter, and the permanently snow-covered location at Greenland. For these locations, the number of PCs was chosen to reconstruct high spectral emissivity spectra. The reconstructed spectra were subsequently compared to laboratory measurements or other in situ measurements. More details about the validation are provided in Part 2 of this paper [32].

The left panels of Figure 9 show the number of PCs that were chosen for the three lab datasets, as well as the optimal number of PCs that were determined where the PCV value equaled 0.999. The right panels illustrate the eigenvalues of the laboratory datasets. The nature of the eigenvalues becomes less significant after the first eight eigenvectors for Version 8 and Version 10, and after two eigenvectors for Version 12, which indicates that the optimal number of PCs can be as low as nine for Version 8 and Version 10, and two for Version 12. The optimal number of PCs was then finalized based on inspecting the case studies.

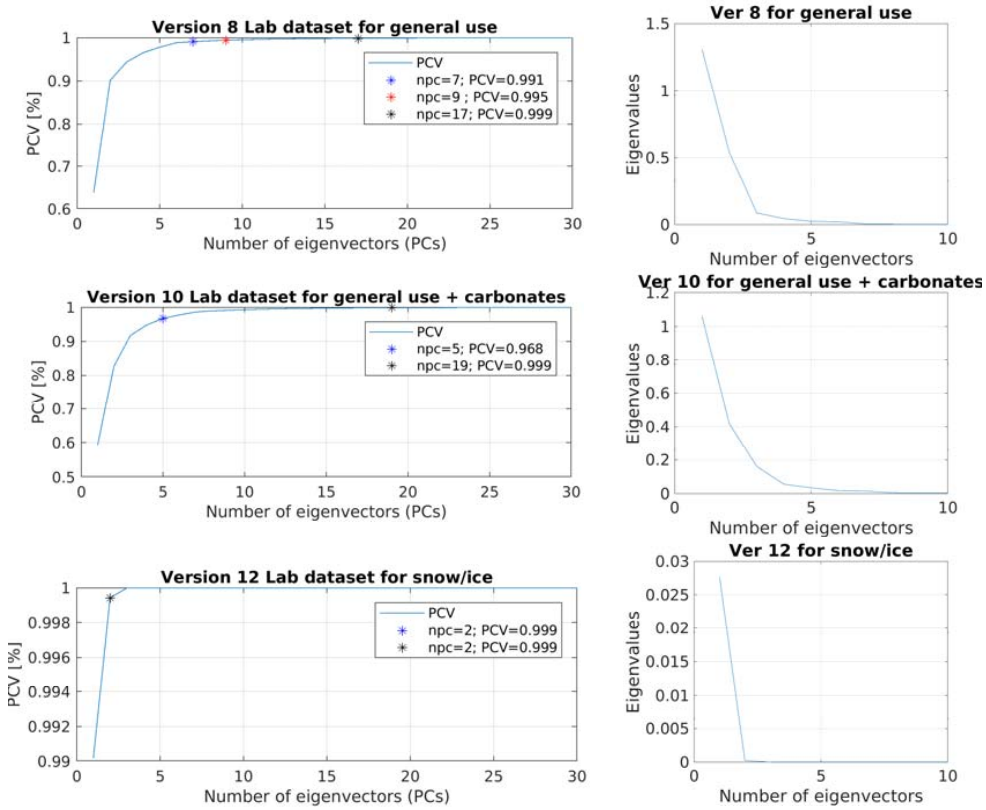

Figure 9. (**Left**) Percentage cumulative variance (PCV) function of the three selected laboratory measurement sets as a function of the number of principal components (PCs). The chosen number of PCs is indicated with blue or red stars. The legend contains the corresponding PCV values. Black stars stand for the number of PCVs, which reached the 0.999 value. (**Right**) The mean eigenvalues of the laboratory datasets for the first 10 eigenvectors.

For example, for the Yemen case (Figure 10a), the optimal number of PCs would be 19 (Figure 9, middle panel), but the emissivity spectra with more than five PCs starts capturing less of the carbonated (dip) feature in the 6–7 μm spectral region. For a general case such as that over the ARM cart site (Figure 10b), the emissivity spectra with seven PCs captures more of the flat shape of the emissivity spectra between the 5–8 μm region than with that nine PCs. However, for the same "general" laboratory set, over the Namib Desert (Figure 10c), nine PCs better captures the quartz doublet feature. For the snow/ice laboratory dataset, the chosen number of PCs is identical with the optimal number of PCs (equal two) determined by the PCV function and eigenvalues (see the bottom panels of Figures 9 and 10d).

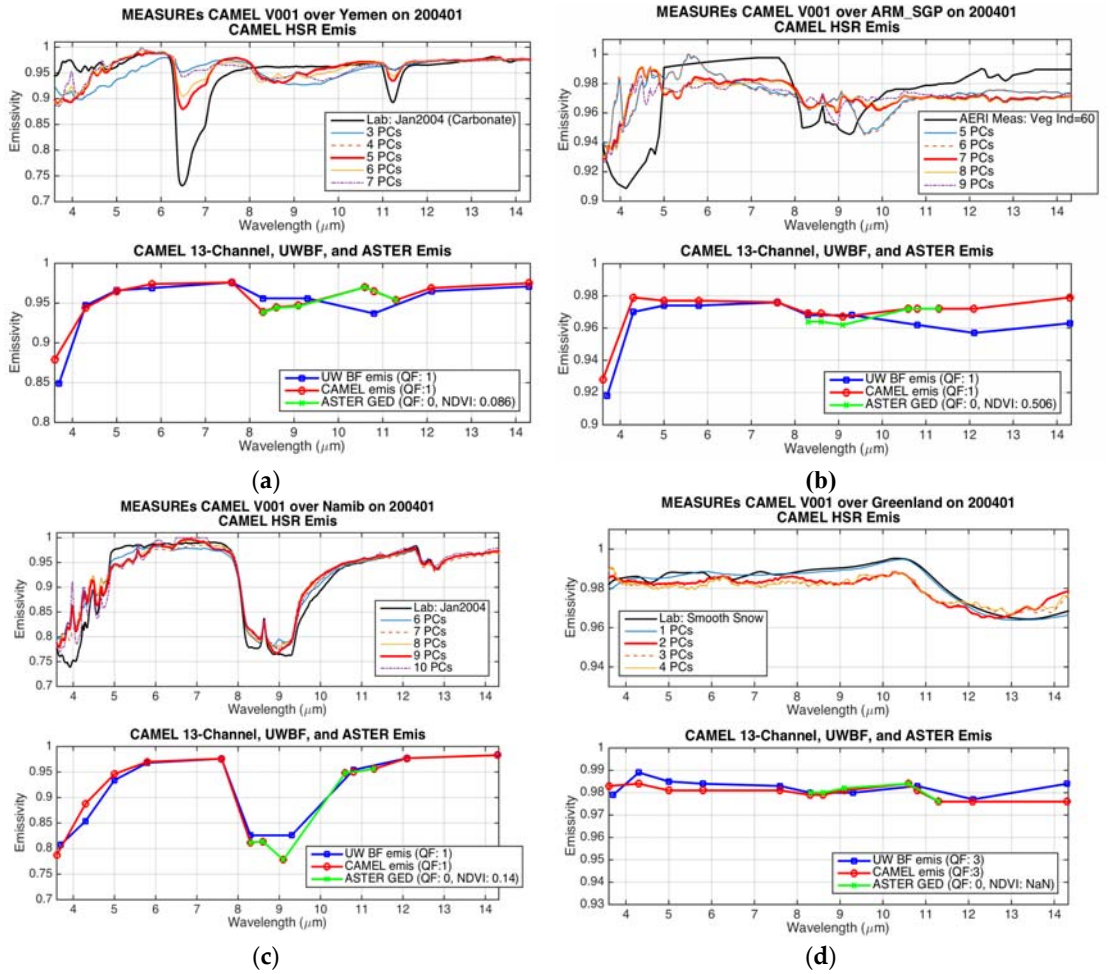

Figure 10. Emissivity on January 2004 at (**a**) Yemen, (**b**) Atmospheric Radiation Measurement (ARM) Southern Great Plains (SGP) Cart site, (**c**) Namib Desert, and (**d**) Greenland case sites. High spectral resolution emissivity from CAMEL with a different number of PCs used (different colored lines) and lab or Atmospheric Emitted Radiance Interferometer (AERI) measurements (black) are shown in the top row panels. The selected number of PCs is solid red for each case.

4. CAMEL Products

As noted earlier, the CAMEL dataset includes monthly global records of emissivity and uncertainty at 13 hinge points between 3.6–14.3 μm, as well as PCA coefficients at 5-km resolution for the years 2000 to 2016. A HSR algorithm is also provided for HSR applications. Detailed information about these file specifics is provided in the CAMEL Users' Guide [33].

The input UW BF emissivity database of the CAMEL dataset is based on the Aqua/MODIS MYD11 monthly mean emissivity product. For the time period between 2000 and 2002, when the

Aqua satellite was not yet launched, the Terra/MODIS MOD11C3 monthly mean emissivities are used to produce the UW BF data, which are subsequently input to the CAMEL database. To check the data consistency and continuity of the Aqua and Terra MODIS, time series of CAMEL, ASTER, Aqua/MODIS MYD11, and Terra/MODIS MOD11 are compared over four case study sites. Figure 11 demonstrates unbiased and consistent agreement between Aqua and Terra MOD11 products over a Rocky Mountain case site for five common wavelengths. The peaks in the CAMEL products during the winter months reflect the snow cover over the area.

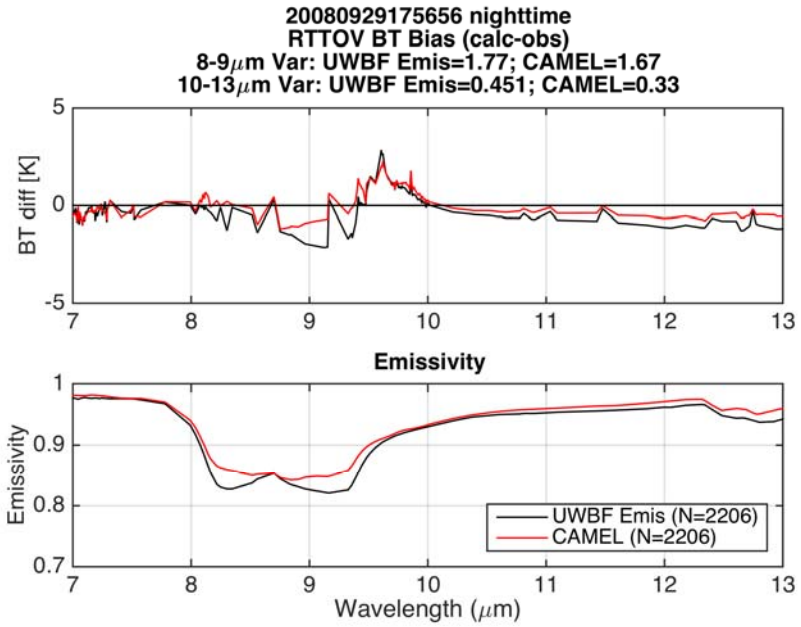

Figure 11. The CAMEL dataset is currently available for the years 2003–2015, and makes use of the Aqua MODIS data as input to the 13 hinge-point product. The dataset is now extended to 2000, and uses the Terra MODIS data for the months of 2000 through December 2002. Time series of the CAMEL, ASTER GEDv4, UW BF (UW BF), and MODIS emissivity are shown, and demonstrate consistency between the Aqua and Terra products over the Rocky Mountain case site.

The CAMEL emissivity products also include the MOD10 snow fraction, the ASTER NDVI, and a quality flag for each pixel. The CAMEL quality flag is determined based on the quality flags of the two input datasets (see Table 3). It ranges from 1 as the best quality to 4 as the least confident quality product. The quality values 2, 3, and 4 indicate when either UW BF, ASTER GEDv4, or both are filled from nearby valid grid cell estimates or from the average value of the neighboring months or yearly data. The quality flag can also be used as a sea/land mask. A zero value means sea or inland water, while a non-zero value is over land.

Table 3. Definition of the CAMEL emissivity quality flag.

Value	Description
0	sea or inland water
1	input UW BF and ASTER GEDv4 data are good quality
2	input UW BF is good quality and ASTER GEDv4 is filled
3	the input UW BF is filled, but ASTER GEDv4 is good quality
4	both the UW BF and ASTER GEDv4 values are filled

The product uncertainty is estimated by a total emissivity uncertainty comprised of three independent components: temporal, spatial, and algorithm variability. Each measure of uncertainty is provided for all 13 hinge points and at every latitude–longitude point. The total uncertainty is

calculated from the components as a root square sum. Part 2 of this paper [32] provides detailed information on how each component is determined.

5. Applications

Within the NASA MEaSUREs LST&E project, the surface emissivity product plays a critical role in the estimating of surface skin temperature derived from satellite remote sensing [33]. In particular, the intent of the MEaSUREs LST&E project is to unify the global LST estimates from polar orbiting and geostationary satellites through the use of a common emissivity database. Another important application of the CAMEL emissivity database is for medium range weather forecasting, where variability in land surface emissivity has led to the blacklisting (i.e., neglect) of infrared satellite measurements that are not accurately represented by the forecast model, i.e., due to a lack of knowledge of land surface properties [34]. In numerical weather prediction (NWP), the surface emissivity contributes to both the land surface model and the assimilation of satellite infrared radiance channels.

NWP land surface models attempt to model the diurnal variation of surface air temperature using a broadband radiative balance between incoming short-wave heating and long-wave cooling [35]. Due to a prior lack of spatially and temporally variant global broadband emissivity (BBE) measurements, it has been common practice in land surface models to set BBE as a single constant for all land types. This may lead to systematic biases in the estimated net radiation for any particular location and time. The CAMEL HSR product provides an opportunity to create a monthly mean BBE product [36] by numerical integration over the CAMEL spectrum. Initial investigations show that improved estimates of variations over time and land cover classification are more realistic when using BBE derived from the CAMEL dataset [37].

An accurate emissivity is also required for any application involving calculations of brightness temperatures, such as the assimilation of radiances into global weather (or climate) models. For example, an interface to the HSR emissivity algorithm with the emissivity database was implemented into the European Organization for the Exploitation of Meteorological Satellites (EUMETSAT) Numerical Weather Prediction Satellite Application Facilities (NWP SAF) Radiative Transfer for Television Infrared Observation Satellites (TIROS) Operational Vertical Sounder (RTTOV) model Version 10 (UWIREMIS) and 12 (CAMEL). The implementation, testing, and evaluation of that HSR emissivity module is described in Borbas and Ruston [11]. The RTTOV model [38] is the primary tool used at the Met Office in the United Kingdom (UK) and European Centre for Medium-range Weather Forecasting (ECMWF) for the assimilation of high spectral resolution infrared sounders, including the NASA Aqua AIRS, the EUMETSAT Meteorological Operational Satellite (METOP) Infrared Atmospheric Sounding Interferometer (IASI), and the Suomi National Polar-orbiting Operational Environmental Satellite System (NPOESS) Preparatory Project (S-NPP)/NOAA-20 Cross-track Infrared Sounder (CrIS) sensors. The surface emissivity is used to provide the boundary condition for computing the upwelling radiance from the surface. Spectral errors in surface emissivity can lead to misinterpretation of the IR observations and errors in the derived air temperature or moisture profiles. Table 4 includes a summary of the main differences between the RTTOV Version 10 and Version 12 land surface IR emissivity modules, e.g., the different input datasets and spatial resolution. The CAMEL module kept the original $0.05^\circ \times 0.05^\circ$, while the UWIREMS module was degradated to $0.1^\circ \times 0.1^\circ$ spatial resolution. In addition, the new CAMEL module uses three laboratory datasets, with various numbers of PCs based on surface scene and coverage, as described in Section 3.2.

Table 4. Summary of comparison between the RTTOV10/UWIREMIS and RTTOV12/CAMEL emissivity databases.

	RTOV10/UWIREMIS	RTTOV12/CAMEL
Spatial Resolution:	0.1° × 0.1°	0.05° × 0.05°
Inputs:	MODIS MYD11 (6) MODIS-ASTER Lab	UW BF (10) ATER-GEDv4 (5) MODIS-ASTER Lab
Method:	Baseline-fit conceptual modelPCA regression	Conceptual hinge-points method PCA regression
Laboratory data:	One set of 123 selected MODIS/ASTER	three sets of MODIS/ASTER: 55 general set; 82 general + carbonates; 4 ice/snow
Number of PCs	6	2, 5, 7, or 9 depends on surface types, $ASTER_{8.6}$ emis & NDVI, MOD10 snow fraction
Outputs	Emissivity spectra on 10 hinge points and 417 HSR points, PCA coefficients	Emissivity spectra on 13 hinge points and 417 HSR points, PCA coefficients, uncertainties, NDVI, snow fraction

The geographical locations where significant improvements are expected in RTTOV performance using the CAMEL module in Version 12 versus the UWIREMIS module in Version 10 are over snow/ice surfaces and non-vegetated surfaces including bare soil, sand, and rock (including quartz and carbonates). To ascertain these improvements, IASI observed brightness temperatures were compared to those calculated using the RTTOV UW IR emissivity (UWIREMIS) module based on (1) the UW BF, and (2) the NASA MEaSUREs CAMEL database. The debiased variances over the 3.6–5 μm, 8–9 μm, and 10–13 μm spectral region are calculated and used as the indicator for an improved emissivity estimate. Figures 12 and 13 illustrate an IASI granule at 17:56 UTC on 29 September 2008, where the CAMEL emissivity improves the brightness temperature calculations over the Arabian Peninsula. The full results of the RTTOV simulation study is reported in Part 2 of this paper [32].

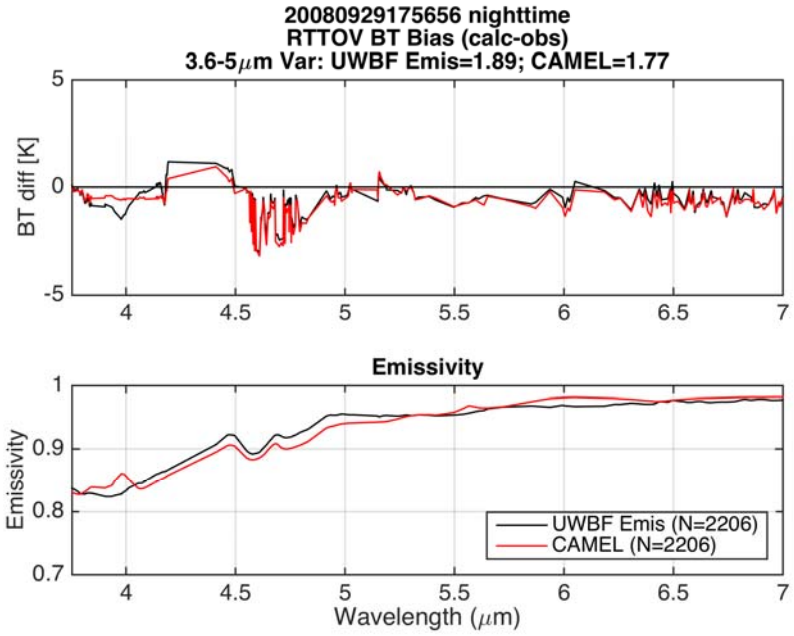

Figure 12. IASI observed brightness temperatures are compared to those calculated using the Radiative Transfer for TOVS (RTTOV) UW IR emissivity module based on the UW BF emissivity database (black) and the CAMEL emissivity database (red) for the granule at 17:56 UTC, on 29 September 2008. The debiased variances are included over the 8–9 μm and 10–13 μm spectral regions.

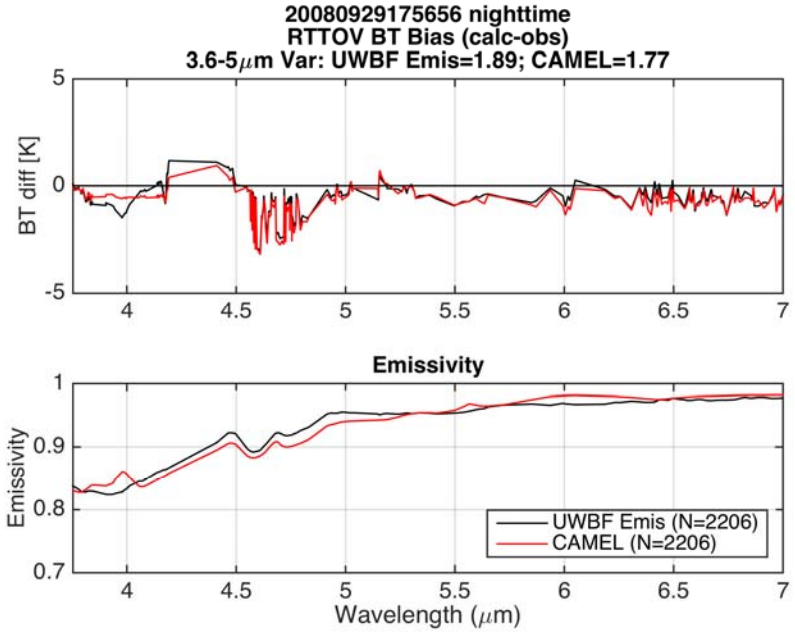

Figure 13. Same as Figure 12 but for the short IR spectral region (between 3.6–7 μm).

A related near-real time application of the CAMEL emissivity is to improve the training sets used to derive the temperature and moisture profiles from the high spectral resolution sounders [39]. The advantage of using the CAMEL database in a retrieval algorithm as a first guess and also in the training phase is demonstrated for the EUMETSAT IASI Algorithm [40]. Similar studies are underway at NOAA for application to the operational CrIS sensor with an emphasis on trace gas retrievals over land [41].

6. Conclusions and Future Plans

The CAMEL database was created by merging the UW MODIS-based emissivity database (UW BF) developed at the University of Wisconsin-Madison, and the ASTER Global Emissivity Dataset Version 4 produced at JPL. The new CAMEL database is integrated to capitalize on the unique strengths of each product's characteristics. The CAMEL ESDR includes monthly global records of emissivity and related uncertainties at 13 hinge points between 3.6 and 14.3 μm, as well as PCA coefficients at 5-km resolution for the years 2000 through 2016. A HSR algorithm has been developed for HSR applications, such as in data assimilation schemes and radiative transfer models that require accurate high spectral resolution emissivity as a first guess for hyperspectral resolution retrieval schemes such as those for AIRS, IASI, and CrIS. This paper describes the 13 hinge-point combination methodology and the high spectral resolution algorithm, and reports on the current status of the dataset. The CAMEL products are evaluated extensively with laboratory measurements over different field sites, with IASI climatological data [42] and using the RTTOV forward model for IASI brightness temperature simulation. Part 2 [32] of this paper provides more information about the results of these validations and evaluations.

The input of the UW BF dataset required for producing CAMEL is the MODIS MOD11C3 monthly mean emissivity products, which includes emissivity at six IR bands. The climate quality of the UW BF dataset is affected by changes over time in the quality of the MOD11 products. In 2017, the processing of the MOD11C3 Col 4.1/5 product was discontinued and replaced by a new Col6 product with some major differences and consequences for CAMEL. The discontinuation of the Col4.1/5 MOD11C3 products and a bug in the Col6 products requires a transition to the new MOD21 emissivity products developed by JPL, which will soon be available. We anticipate that the transition from MOD11 to MOD21 for CAMEL Version 2 will improve the product accuracy and reduce the systematic and time-dependent errors that have been identified in CAMEL Version 1 (V1).

In CAMEL V1, a distinct set of laboratory measurements (including snow and ice spectra) are uniquely assigned to snow-covered areas. The snow emissivity that was derived using the unique snow/ice emissivity spectra is calculated for 5 km × 5 km pixels where the snow fraction (derived from MOD10) is >0.5. This is not optimal for pixels covered partially by snow. In the future, we plan to determine the emissivity as a linear blend of the snow and underlying land emissivity values weighted by the observed snow fraction. This should lead to improvements in high latitude forest regions and in transition zones at mid-latitudes.

The MOD11 emissivity product input to CAMEL uses a day/night algorithm with the assumption that day and night emissivity does not change over a period of a few days. That inherent assumption could introduce an error, such as if, for example, the day/night emissivity changes due to soil moisture, snowmelt, or any rapid changes in surface (e.g., fire). However, this error is very difficult to quantify, and there are no uncertainty estimates of this provided in the original MODC3 products developed by Wan et al. [27]. Masiello et al. [25] used IASI observations, and Li et al. [43] used geostationary satellite data over the Sahara Desert to show that the IR emissivity between 8.7–12 μm has a diurnal variation. The strongest diurnal effect occurs at 8.7 μm, with the highest value at night and the lowest value during the day. The diurnal effect is the weakest at 12 μm, with an opposite feature. The assumption of equal day–night emissivity can result in as much as a 2% emissivity error at 8.7 μm over desert. In future work, we plan to investigate whether there is a diurnal effect in the MODIS product, and how much it contributes to CAMEL uncertainties.

The CAMEL V1 does not yet include an angular dependence to the emissivity. However, laboratory measurement studies [44–46] show an angular variation in thermal IR emissivity in the 8–14 μm spectral band for non-vegetated soils and samples, while homogeneous grass, for example, does not show a strong angular dependence. Garcia-Santos et al. [47] and Ruston et al. [48] found that the emissivity change is small for viewing angles lower than 40°, but at higher viewing angles, the emissivity decreased significantly. Garcia-Santos et al. established a relationship to take into account the viewing zenith angle dependencies for a range of soil types. In contrast to the bare soils, vegetated surfaces can exhibit a "canopy" effect where the emissivity value actually increases along with the viewing angle. Borbas et al. [49], under a EUMETSAT NWP-SAF Associate Scientist Mission, investigated the angular dependence of the IR emissivity using satellite retrieved measurements over the IR spectrum derived from the CrIS as a function of International Geosphere-Biosphere Programme (IGBP) ecosystem types, wavelengths, and seasons. The difference between the mean emissivity at nadir (0°) and the maximum of 60° shows a 6.8% and 8.0% increase at 3.7 μm and 4.3 μm, respectively, during daytime, and 3.2% and 6.4% during nighttime. Over the TIR region, the land surface emissivity does not vary much, so the angular changes are much smaller as well. Decreases of 1.1% and 0.9% in emissivity were observed at 12.1 μm. We are planning to develop a parameterization correction/function for angle dependence, which will be incorporated into the CAMEL algorithm uncertainty based on results from Garcia-Santos et al. [47] and Ruston et al. [48]. Our goal is to provide improved uncertainty estimates for high viewing angles based on these results, which will help promote the use of improved climate quality products for all view angle geometry configurations.

The CAMEL database unifies the infrared emissivity measurements from NASA sensors under the umbrella of a NASA MEASURES LST&E project. The CAMEL dataset is expected to decrease the errors in LST estimation from moderate spatial resolution satellites by providing realistic surface emissivity estimates with global coverage and monthly temporal sampling at 5-km resolution. Applications to NWP short and medium range weather forecasting are in progress, with the potential for climate applications as the emissivity record is extended in time using NOAA satellites.

Author Contributions: E.B., G.H. and R.K. conceived and designed the method; M.F. analyzed the data; S.H. contributed his expertise; E.B. wrote the paper.

Acknowledgments: This research was supported by the NASA grant NNX08AF8A. The MODIS MOD10, MOD11, MYD11, MOD13, ASTER GED Version 4 and CAMEL Version 1 products used in this study are available courtesy of the NASA EOSDIS Land Processes Distributed Active Archive Center (LP DAAC), United States Geological Survey/Earth Resources Observation and Science Center, Sioux Falls, South Dakota, [https://lpdaac.usgs.gov/dataset_discovery/aster].

Conflicts of Interest: The authors declare no conflict of interest.

References

1. Willet, K.; Thorne, P. The ISTI Steering Committee. Progress Report for the International Surface Temperature Initiative. 2011. Available online: http://www.surfacetemperatures.org/progress_reports (accessed on 15 November 2017).
2. Anderson, M.C.; Norman, J.M.; Mecikalski, J.R.; Otkin, J.A.; Kustas, W.P. A climatological study of evapotranspiration and moisture stress across the continental United States based on thermal remote sensing: 2. Surface moisture climatology. *J. Geophys. Res. Atmos.* **2007**, *112*. [CrossRef]
3. Moran, M.S. Thermal infrared measurement as an indicator of plant ecosystem health. In *Thermal Remote Sensing in Land Surface Processes*; Quattrochi, D.A., Luvall, J., Eds.; Taylor and Francis: Abingdon-on-Thames, UK, 2003; pp. 257–282.
4. Zhou, L.; Dickinson, R.E.; Tian, Y.; Jin, M.; Ogawa, K.; Yu, H.; Schmugge, T. A sensitivity study of climate and energy balance simulations with use of satellite-derived emissivity data over Northern Africa and the Arabian Peninsula. *J. Geophys. Res. Atmos.* **2003**, *108*, 4795. [CrossRef]
5. French, A.N.; Schmugge, T.J.; Ritchie, J.C.; Hsu, A.; Jacob, F.; Ogawa, K. Detecting land cover change at the Jornada Experimental Range, New Mexico with ASTER emissivities. *Remote Sens. Environ.* **2008**, *112*, 1730–1748. [CrossRef]
6. Seemann, S.W.; Li, J.; Menzel, W.P.; Gumley, L.E. Operational retrieval of atmospheric temperature, moisture, and ozone from MODIS infrared radiances. *J. Appl. Meteorol.* **2003**, *42*, 1072–1091. [CrossRef]
7. Hulley, G.; Hook, S. *MOD21 MODIS/Terra Land Surface Temperature/3-Band Emissivity 5-Min L2 1 km V006*; NASA EOSDIS Land Processes DAAC: Sioux Falls, SD, USA, 2017. [CrossRef]
8. Hulley, G.; Hook, S. *AG100: ASTER Global Emissivity Dataset 100-meter V003*; NASA EOSDIS Land Processes DAAC; USGS Earth Resources Observation and Science (EROS) Center: Sioux Falls, SD, USA, 2014. [CrossRef]
9. Borbas, E.; Seemann, S.W. *Global Infrared Land Surface Emissivity: UW-Madison Baseline Fit Emissivity Database V2.0*; Space Science and Engineering Center, University of Wisconsin-Madison: Madison, WI, USA, 2007. Available online: http://cimss.ssec.wisc.edu/iremis/ (accessed on 15 November 2017).
10. Hulley, G.; Hook, S. *AG5KMMOH: ASTER Global Emissivity Dataset, Monthly, 0.05 degree, HDF5 V041*; NASA EOSDIS Land Processes DAAC, USGS Earth Resources Observation and Science (EROS) Center: Sioux Falls, SD, USA, 2016. [CrossRef]
11. Borbas, E.E.; Ruston, B.C. *The RTTOV UW IR Land Surface Emissivity Module. Mission Report NWPSAF-MO-VS-042*; EUMETSAT Numerical Weather Prediction; Satellite Applications Facility: Darmstadt, Germany, 2010. Available online: nwpsaf.eu/vs_reports/nwpsaf-mo-vs-042.pdf (accessed on 15 November 2017).
12. Hook, S. *CAM5K30EM: Combined ASTER and MODIS Emissivity for Land (CAMEL) Emissivity Monthly Global 0.05 Deg V001*; NASA EOSDIS Land Processes DAAC, USGS Earth Resources Observation and Science (EROS) Center: Sioux Falls, SD, USA, 2017. [CrossRef]
13. Hulley, G.C.; Hook, S.J. Generating Consistent Land Surface Temperature and Emissivity Products Between ASTER and MODIS Data for Earth Science Research. *IEEE Geosci. Remote Sens. Lett.* **2010**, 1304–1315. [CrossRef]
14. Hulley, G.; Hook, S.J.; Abbott, E.; Malakar, N.; Islam, T.; Abrams, M. The ASTER Global Emissivity Dataset (ASTER GED): Mapping Earth's emissivity at 100 meter spatial resolution. *Geophys. Res. Lett.* **2015**, *42*. [CrossRef]
15. Hulley, G.C.; Hook, S.J. Intercomparison of Versions 4, 4.1 and 5 of the MODIS Land Surface Temperature and Emissivity Products and Validation with Laboratory Measurements of Sand Samples from the Namib Desert, Namibia. *Remote Sens. Environ.* **2009**, *113*, 1313–1318. [CrossRef]

16. Hulley, G.C.; Hook, S.J. The North American ASTER Land Surface Emissivity Dataset (NAALSED) Version 2.0. *Remote Sens. Environ.* **2009**, *113*, 1967–1975. [CrossRef]
17. Vogel, R.; Liu, Q.; Han, Y.; Weng, F. Evaluating a satellite-derived global infrared land surface emissivity data set for use in radiative transfer modeling. *J. Geophys. Res. Atmos.* **2011**, *116*, 11. [CrossRef]
18. Gutman, G.; Ignatov, A. The derivation of the green vegetation fraction from NOAA/AVHRR for use in numerical weather prediction models. *Int. J. Remote Sens.* **1998**, *19*, 1533–1543. [CrossRef]
19. Knuteson, R.O.; Best, F.A.; DeSlover, D.H.; Osborne, B.J.; Revercomb, H.E.; Smith, W.L., Sr. Infrared land surface remote sensing using high spectral resolution aircraft observations. *Adv. Space Res.* **2004**, *33*, 1114–1119. [CrossRef]
20. Abrams, M. (NASA/JPL). Personal Communication, 2018.
21. Wolfe, R.E.; Nishihama, M.; Fleig, A.J.; Kuyper, A.; Roy, P.; Storey, J.C.; Patt, F.S. Achieving sub-pixel geolocation accuracy in support of MODIS land science. *Remote Sens. Environ.* **2002**, *83*, 31–49. [CrossRef]
22. Lin, G.; Wolfe, R.; Kuyper, J.; Yin, Z.; Tan, B. *(Terra, Aqua) MODIS Geolocation Status*; NASA GSFC Code 619; MODIS Science Team Meeting, Calibration Workshop: Greenbelt, MD, USA, 2016. Available online: https://modis.gsfc.nasa.gov/sci_team/meetings/201606/presentations/cal/MODIS_VIIRS_Geolocation_Status_CalWorkshop_Lin_2016.pdf (accessed on 15 February 2018).
23. Moeller, C. (UW-Madison/SSEC). Personal Communication, 2018.
24. Seemann, S.W.; Borbas, E.E.; Knuteson, R.O.; Stephenson, G.R.; Huang, H.L. Development of a global infrared land surface emissivity database for application to clear sky sounding retrievals from multispectral satellite radiance measurements. *J. Appl. Meteorol. Climatol.* **2008**, *47*, 108–123. [CrossRef]
25. Masiello, G.; Serio, C.; Venafra, S.; DeFeis, I.; Borbas, E.E. Diurnal variation in Sahara desert sand emissivity during the dry season from IASI observations. *J. Geophys. Res. Atmos.* **2014**, *119*, 1626–1638. [CrossRef]
26. Baldridge, A.M.; Hook, S.J.; Grove, C.I.; Rivera, G. The ASTER Spectral Library Version 2.0. *Remote Sens. Environ.* **2009**, *114*, 711–715. [CrossRef]
27. Wan, Z.M.; Li, Z.L. A physics-based algorithm for retrieving land-surface emissivity and temperature from EOS/MODIS data. *IEEE Trans. Geosci. Remote Sens.* **1997**, *35*, 980–996.
28. MODIS Land Surface Emissivity/Temperature (MOD11) C4.1 LST Document. Available online: http://landweb.nascom.nasa.gov/QA_WWW/forPage/C41_LST.doc (accessed on 15 February 2018).
29. Wilson, T.; Wu, A.; Geng, X.; Wang, Z.; Xiong, X. Analysis of the electronic crosstalk effect in Terra MODIS long-wave infrared photovoltaic bands using lunar images. *Image Signal Process. Remote Sens.* **2016**, *22*, 100041C.
30. Salisbury, J.W.; D'Aria, D.M. Emissivity of terrestrial materials in the 8-14 μm atmospheric window. *Remote Sens. Environ.* **1992**, *42*, 83–106. [CrossRef]
31. Salisbury, J.W.; D'Aria, D.M. Emissivity of terrestrial materials in the 3-5 μm atmospheric window. *Remote Sens. Environ.* **1994**, *47*, 345–361. [CrossRef]
32. Feltz, M.; Borbas, E.; Knuteson, R.; Hulley, G.; Hook, S.J. The Combined ASTER MODIS Emissivity Over Land (CAMEL) Part 2: Uncertainty and Validation. *Remote Sens.* **2018**, under review.
33. Borbas, E.; Hulley, G.; Knuteson, R.; Feltz, M. MEaSUREs Unified and Coherent Land Surface Temperature and Emissivity (LST&E) Earth System Data Record (ESDR): The Combined ASTER and MODIS Emissivity Database over Land (CAMEL) Users' Guide; 2017. Available online: https://lpdaac.usgs.gov/sites/default/files/public/product_documentation/cam5k30_v1_user_guide_atbd.pdf (accessed on 15 November 2017).
34. Dee, D.P.; Uppala, S.M.; Simmons, A.J.; Berrisford, P.; Poli, P.; Kobayashi, S.; Andrae, U.; Balmaseda, M.A.; Balsamo, G.; Bauer, P.; et al. The ERA-Interim reanalysis: Configuration and performance of the data assimilation system. *Q. J. R. Meteorol. Soc.* **2011**, *137*, 553–597. [CrossRef]
35. Reichle, R.H.; Sujay, V.K.; Sarith, P.P.M.; Randal, D.K.; Liu, Q. Assimilation of satellite-derived skin temperature observations into land surface models. *J. Hydrometeorol.* **2010**, *11*, 1103–1122. [CrossRef]
36. Borbas, E.; Feltz, M.; Knuteson, R. *Broad Band Emissivity Derived from the MEaSUREs CAMEL V001 Database*; UW-Madison, Space Science and Engineering Center: Madison, WI, USA, 2017. Available online: https://doi.org/10.21231/S2PP8H (accessed on 15 November 2017).

37. Feltz, M.; Borbas, E.; Knuteson, R.; Hulley, G.; Hook, S. Global Broadband IR Surface Emissivity Computed from Combined ASTER and MODIS Emissivity over Land (CAMEL). In Proceedings of the American Meteorological Society Joint 21st Satellite Meteorology, Oceanography and Climatology Conference and 20th Conference on Air-Sea Interaction, Madison, WI, USA, 15–19 March 2016. Available online: https://ams.confex.com/ams/21SATMET20ASI/webprogram/Paper296752.html (accessed on 15 February 2018).
38. Saunders, R.; Hocking, J.; Rundle, D.; Rayer, P.; Havemann, S.; Matricardi, M.; Geer, A.; Cristina, L.; Brunel, P.; Vidot, J. RTTOV-12 Science and Validation Report; NWPSAF-MO-TV-41; 2017. Available online: https://www.nwpsaf.eu/site/download/documentation/rtm/docs_rttov12/rttov12_svr.pdf (accessed on 15 February 2018).
39. Weisz, E.; Smith, W.L.; Smith, N. Advances in simultaneous atmospheric profile and cloud parameter regression based retrieval from high-spectral resolution radiance measurements. *J. Geophys. Res. Atmos.* **2013**, *118*, 6433–6443. [CrossRef]
40. August, T. The EUMETSAT operational IASI L2 products and services, from Global to Regional. In Proceedings of the International TOVS Study Conference, Darmstadt, Germany, 29 November–5 December 2017.
41. Gambacorta, A.; Barnet, C.; Wolf, W.; King, T.; Maddy, E.; Strow, L.; Xiong, X.; Nalli, N.; Goldberg, M. An Experiment Using high spectral resolution CrIS measurements for atmospheric trace gases: Carbon monoxide retrieval impact study. *IEEE Geosci. Remote Sens. Lett.* **2014**, *11*, 1639–1643. [CrossRef]
42. Zhou, D.; Larar, M.A.; Liu, X.; Smith, W.; Strow, L.; Yang, P.; Schluessel, P.; Calbet, X. Global Land Surface Emissivity Retrieved From Satellite Ultraspectral IR Measurements. *IEEE Trans. Geosci. Remote Sens.* **2011**, *49*, 1277–1290. [CrossRef]
43. Li, Z.; Li, J.; Li, Y.; Zhang, Y.; Schmit, T.J.; Zhou, L.; Goldberg, M.D.; Menzel, W.P. Determining diurnal variations of land surface emissivity from geostationary satellites. *J. Geophys. Res.* **2012**, *117*, D23302. [CrossRef]
44. Label, J.; Stoll, M.P. Angular variation of land surface spectral emissivity in the thermal infrared: Laboratory investigations on bare soils. *Int. J. Remote Sens.* **1991**, *12*, 2299–2310.
45. Sobrino, J.A.; Cuenca, J. Angular variation of thermal infrared emissivity for some natural surfaces from experimental measurements. *Appl. Opt.* **1999**, *38*, 3931–3936. [CrossRef] [PubMed]
46. Cuenca, J.; Sobrino, A.J. Experimental measurements for studying angular and spectral variation of thermal infrared emissivity. *Appl. Opt.* **2004**, *43*, 4598–4602. [CrossRef] [PubMed]
47. Garcia-Satnos, V.; Valor, E.; Caselles, V.; Burgos, M.A.; Coll, C. On the angular variation of thermal infrared emissivity of inorganic soils. *J. Geophys. Res.* **2012**, *117*, D19116. [CrossRef]
48. Ruston, B.; Weng, F.; Yan, B. Use of a One-Dimensional variation retrieval to Diagnose Estimates of Infrared and Microwave Surface Emissivity Over Land for ATOVS Sounding Instruments. *IEEE Trans. Geosci. Remote Sens.* **2008**, *46*, 393–402. [CrossRef]
49. Borbas, E.; Investigation into the Angular Dependence of IR Surface Emissivity. Mission Report; EUMETSAT NWPSAF-MO-VS-050; 2014. Available online: https://nwpsaf.eu/vs_reports/nwpsaf-mo-vs-050.pdf (accessed on 15 February 2018).